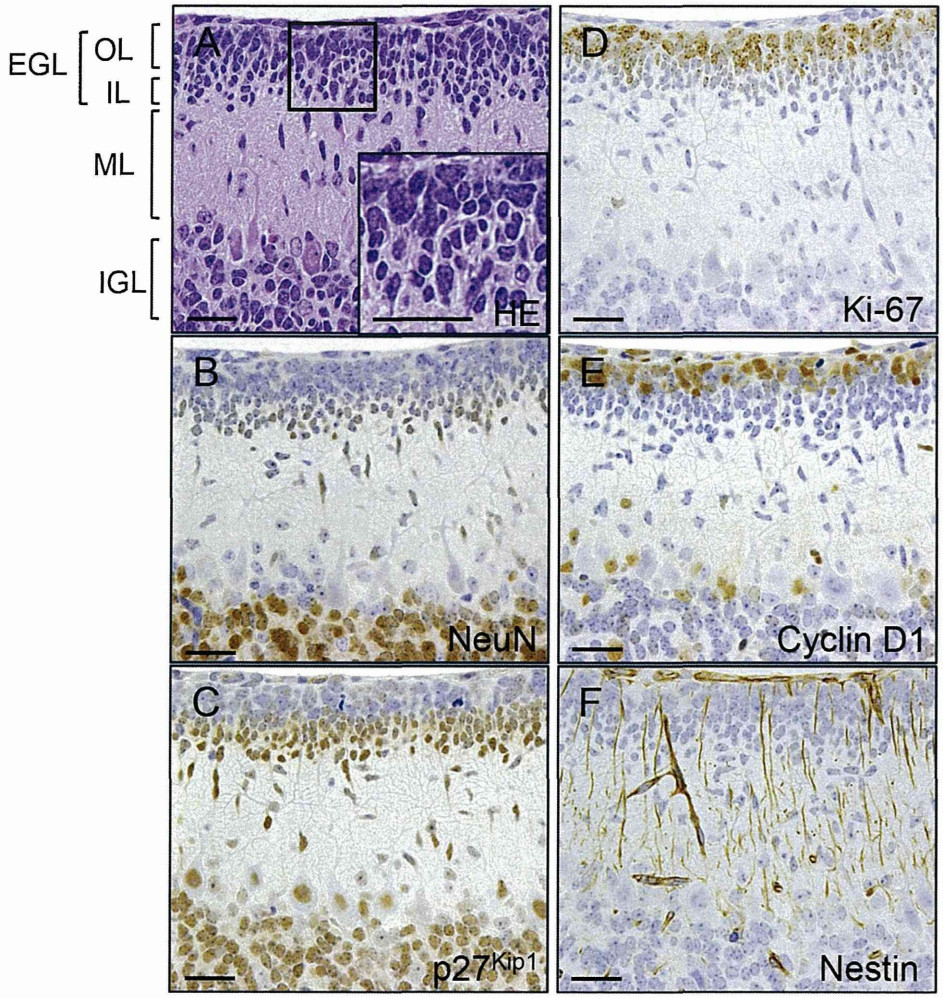

Fig. 5. Morphology and immunohistochemistry of the developing cerebellum. Representative morphology and immunohistochemistry of the developing cerebellar cortex from Ptch1 mice (PND10). Their characteristics were common to both genotypes. (A) HE staining of the cerebellar cortex. EGL framed rectangle was magnified (insert). (B) NeuN was weakly positive in the inner layer of the EGL (IL) and migrating granular cells in the molecular layer (ML) and strongly positive in the IGL. (C) $p27^{kip1}$ was strongly positive in the IL and migrating granular cells in the ML and positive in the IGL. (D) Granular cells in the outer layer of the EGL (OL) were positive for Ki-67. (E) Granular cells in the OL were positive for Cyclin D1. (F) Positive staining for Nestin was observed radically from the surface of the cerebellum to the IGL in a straight line. Scale bars: 25 μm.

and in the abdominal muscles were noted after PND3 in Ptch1 mice only. These intramuscular masses were diagnosed microscopically as rhabdomyosarcomas. Macroscopically, there was no metastatic lesion of MB and rhabdomyosarbomas in tumor-bearing mice.

3.2. Sequential changes in the width and migration process of the EGL

Postnatal changes in the width of the EGL in wild-type and Ptch1 mice are shown in Fig. 2. The width of the EGL peaked at PND4 to 6 and the width in Ptch1 mice was greater than in wild-type mice during first week after birth.

Fig. 3 shows localization of BrdU-positive cells injected in mice at PND8 (Fig. 3A) and PND14 (Fig. 3B), respectively. GCPs in the outer layer of the EGL were the only cell type to be positive for BrdU in the EGL. In animals injected with BrdU at PND8, BrdU-positive cells were observed in the outer layer of the EGL which was positive for Ki-67 1.5 h after the injection (Fig. 3A and 3A inserts). BrdU-positive EGL cells gradually migrated into the IGL accompanied by thinning of the EGL in both genotypes. At PND16, only one layer of the EGL was present and then disappeared at PND21 in both genotypes.

3.3. Sequential changes of Purkinje cells and Bergmann glia in the developing cerebellum

Purkinje cells and Bergmann glia are major components of the cerebellum and have important roles in cerebellar development. Long processes of the radial glial cells, Bergmann glia, were visualized by immunohistochemistry with anti-GFAP antibody (Fig. 4A). For both genotypes, there was no difference in the density or extending direction of the processes at PND0 to 21. In addition, Purkinje neurons (including dendritic arbors) were stained with anti-Calbindin-D-28K antibody (Fig. 4B). From qualitative microscopic inspection a difference in the number, alignment, or arborization of Purkinje cells was not detected between the genotypes during postnatal cerebellar development.

3.4. Morphology and immunohistochemical characteristics of granule cells in the developing cerebellum

Morphology and immunohistochemical reactions to antibodies related to cell proliferation and neuronal differentiation revealed that the structure of the developing cerebellum was common to both genotypes (Table 2 and Fig. 5). Nuclei of GCPs in the outer layer of the EGL were medium to large-sized and round to polygonal. These cells were positive for Ki-67 and Cyclin D1 and negative for

Table 2
Morphological characteristics of granular precursor cells located in EGL, molecular layer, and IGL in developing cerebellum at PND0 to 14.

	EGL		Molecular layer	IGL
	Outer layer	Inner layer		
Histopathology				
	Medium–large size Round–polygonal	Small size Oval–elongate (vertical)	Small size Oval–spindle (vertical)	Medium size Round
Immunohistochemistry				
Ki-67	+	–	–	–
CyclinD1	+	–	–	–
NeuN	–	±	±	+/++
$p27^{kip1}$	–	++	+/++	+
Nestin	+	+	+	$\pm^{a}/-^{b}$

–, negative; ±, weakly positive; +, positive; ++, strongly positive. These characteristics shown in the table are common to all time points measured (PND0 to 14); except for Nestin staining in the IGL.
[a] Until PND10.
[b] Day after PND10.

NeuN and $p27^{kip1}$. Inner layer EGL nuclei were small-sized, oval to elongate, and arranged vertically. In this layer, granular cells were negative for Ki-67 and Cyclin D1, weakly positive for NeuN and strongly positive for $p27^{kip1}$. Migrating granular cells in the molecular layer were oval to spindle shaped small cells arranged vertically and had the same staining profiles as inner layer EGL nuclei. Granular cells with medium-sized round nuclei in the IGL surrounded eosinophilic mossy fibers. Those were negative for Ki-67 and Cyclin D1 and positive to strongly positive for NeuN and $p27^{kip1}$. Positive staining for nestin was observed radically throughout the

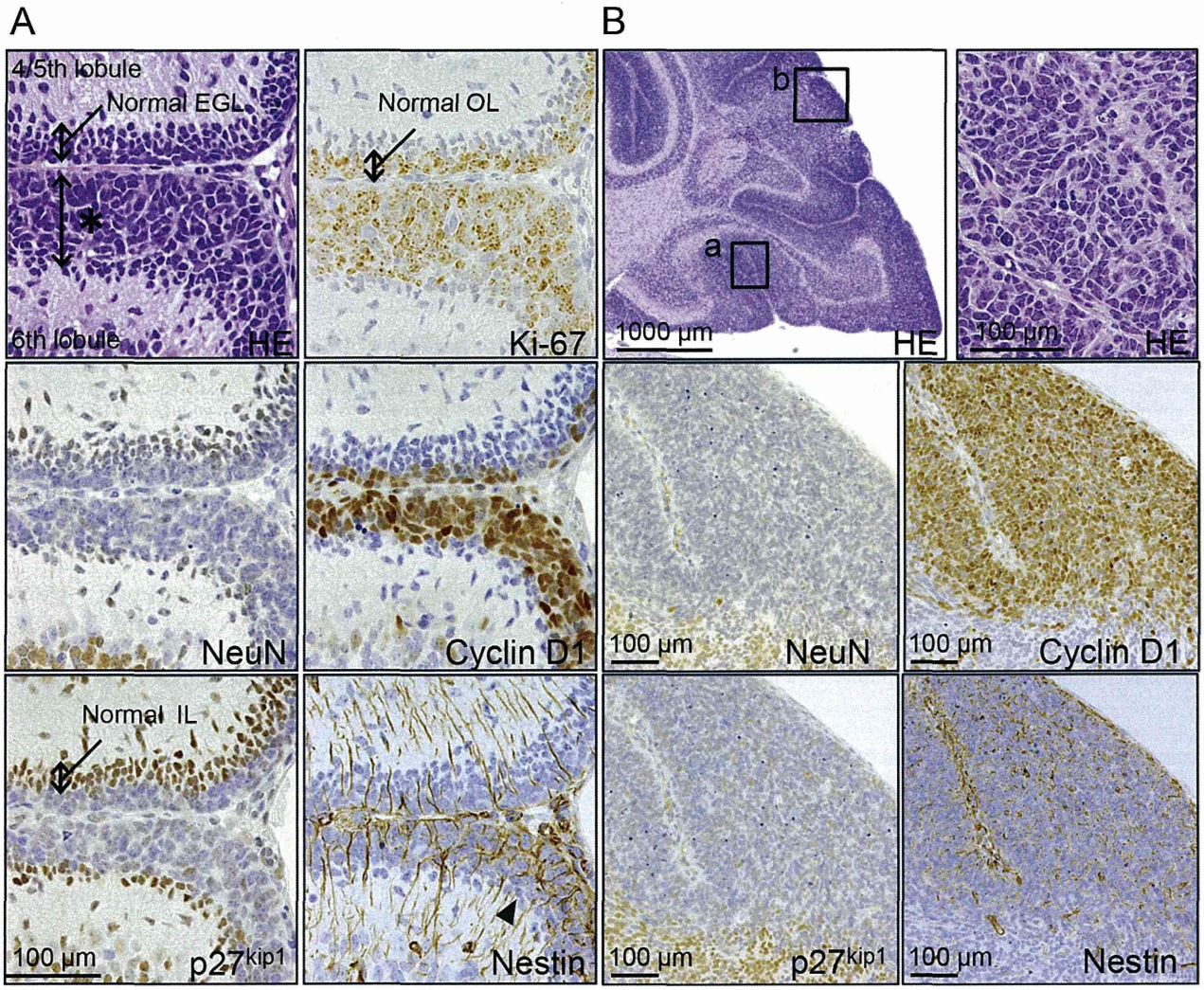

Fig. 6. Proliferative lesions in the developing cerebellum in Ptch1 mice at PND10 and 12. (A) A thickened proliferative lesion (asterisk) in the outer layer of the EGL (6th lobule) in Ptch1 mice at PND10. The 4th/5th lobule showed normal EGL structure. In this lesion, the outer layer of the EGL stained with Ki-67 and cyclinD1 was expanded. The inner layer of the EGL (IL) stained with NeuN and $p27^{kip1}$ was thinned compared to the normal IL in the 4th/5th lobule. Positive staining for Nestin was observed intracellularly in all directions in this lesion (arrowhead). Scale bar: 100 μm. (B) MB in Ptch1 mice at PND12. Higher magnification of rectangle a HE staining showed that proliferating cells resembled thickened lesions of the outer layer of the EGL. The rectangle b showed corresponding area for the pictures stained with NeuN, CyclinD1, $p27^{kip1}$ and Nestin.

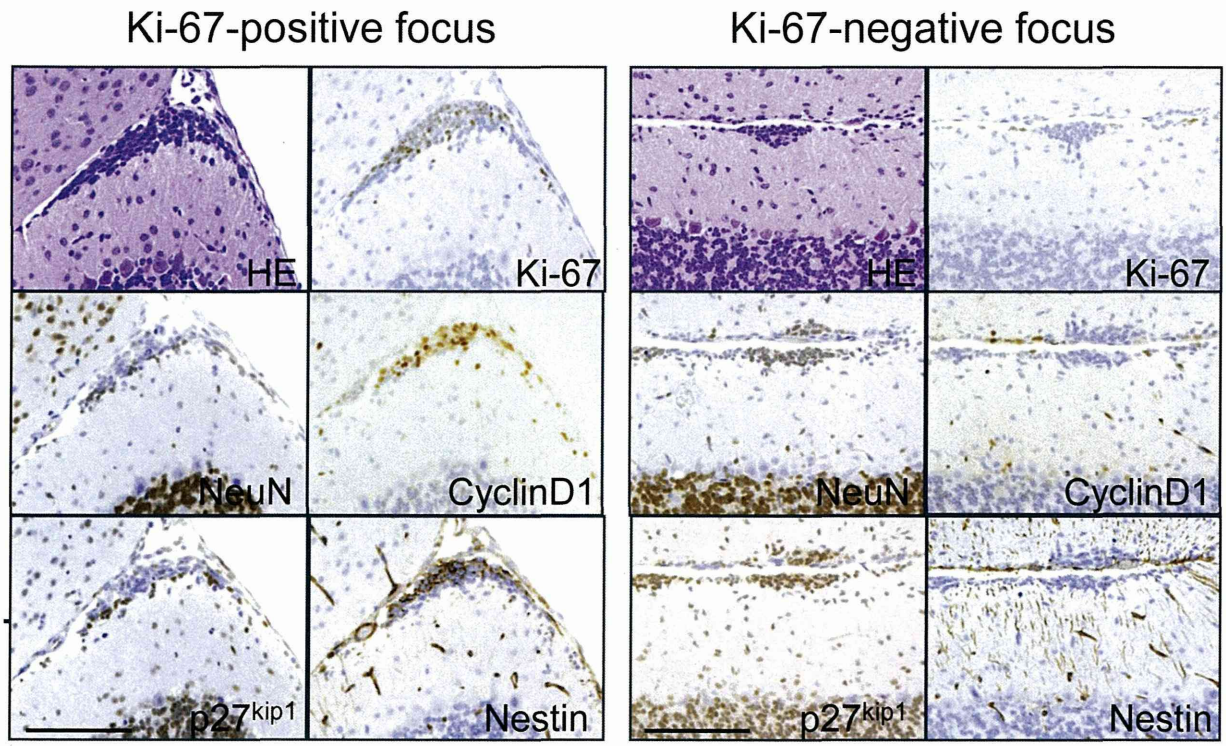

Fig. 7. Immunohistochemical characterization of foci composed of GCP-like cells. Ki-67-positive (left) and Ki-67-negative (right) foci of Ptch1 mice. Ki-67-positive foci were composed of medium to large-sized, round to polygonal nuclei that were negative or weakly positive for NeuN and $p27^{kip1}$ and positive for cyclin D1 and nestin, indicating unclear differentiation into neuronal cells. Ki-67-negative foci were composed of round and small nuclei that were positive for NeuN and $p27^{kip1}$ and negative for Cyclin D1 and nestin, indicating differentiation into neural cells similar to IGL cells. Scale bar: 50 μm.

cerebellar cortex, and weak staining in the IGL remained until PND10.

3.5. Changes in the developing cerebellum and derived cells

Proliferative lesions were observed in the developing cerebellum in Ptch1 mice. Proliferation of GCP-like cells was observed in a thickened area of the EGL, which was continuous from the normal EGL on and after PND10 in Ptch1 mice (Fig. 6A, asterisk). The proliferative lesions substituted for the inner layer of the EGL (Fig. 6A). Moreover, early occurrence of MB was detected at PND12 (Fig. 6B). In both proliferative lesions, large-sized, round to polygonal cells with atypia were main components. Immunohistochemically, the cells were positive for Cyclin D1 and nestin and weakly positive or negative for NeuN and $p27^{kip1}$. Intercellular irregular nestin staining was distinctive of these lesions (Fig. 6A arrowhead and B), as nestin-positive fibers were arranged regularly and radically in a straight line in the normal EGL (Figs. 5F and 6A). Histopathology and immunohistochemistry of these proliferative lesions resembled GCPs in the outer layer of the EGL of the normal cerebellum.

After PND16, the time when migration of EGL cells to the IGL has almost completed, foci with GCP-like cells were detected in the outermost region of the cerebellar cortex in the cerebella of mice from both genotypes (Figs. 3B and 7). In the mice injected with BrdU at PND14, BrdU-positive cells were detected in the EGL 1.5 h after treatment (Fig. 3B) and BrdU-positive cells had migrated into the deep molecular layer and the IGL by PND21 (Fig. 3). As some of the GCP-like cells of the foci in mice injected with BrdU at PND14 were positive for BrdU after PND16, the cells were considered to be derived from the residual GCPs in the EGL (Fig. 3B, arrowhead). The residual foci were clearly classified into two types: Ki-67-positive and Ki-67-negative (Fig. 7). Ki-67-positive foci were composed of atypical cells whose nuclei were medium to large-sized and round to polygonal in shape (Fig. 7, left). The cells were immunohistochemically negative or weakly positive for NeuN and $p27^{kip1}$ and positive for cyclin D1 and nestin (Fig. 7, left). Conversely, Ki-67-negative foci were composed of cells with round and small shaped nuclei. The cells were positive for NeuN and $p27^{kip1}$ and negative for nestin and cyclin D1, indicating differentiation into neural cells (Fig. 7, right). Some of Ki-67-negative foci contained a strongly eosinophilic area resembling mossy fibers among the nuclei (Fig. 8, asterisk) and they were comparable to the structure of the IGL.

3.6. Relationship between residual foci of GCPs and MBs

The incidences of Ki-67-positive or negative foci and MBs were investigated from PND16 up to 10 weeks of age in both genotypes (Fig. 9). MBs were divided into two types: a focal MB occupying one to two lobules of the cerebellum was defined as a small MB and an advanced MB spreading over three or more lobules was defined as a large MB. In Ptch1 mice, Ki-67-positive foci, small MB, and large MB were observed and most of the mice had Ki-67-negative foci. The peak of Ki-67-positive foci was up to PND21, the completion period of cerebellar development. The incidences of MBs were comparable between ages. In wild-type mice, no proliferative lesions, neither Ki-67-positive foci nor MBs other than Ki-67-negative foci, were detected at any age (Fig. 9). The incidence of Ki-67-negative foci decreased with increased age in wild-type mice. The number of Ki-67-negative foci per animal was larger in Ptch1 mice as compared to wild-type mice (data not shown).

Examination for localization of each change revealed that more than 70% of Ki-67-negative foci were localized in the 6–10th lobules of the cerebellum in both genotypes (Fig. 10). In addition, more than 50% of Ki-67-positive foci and small MBs were also observed in the 6–10th lobules in Ptch1 mice (Fig. 10).

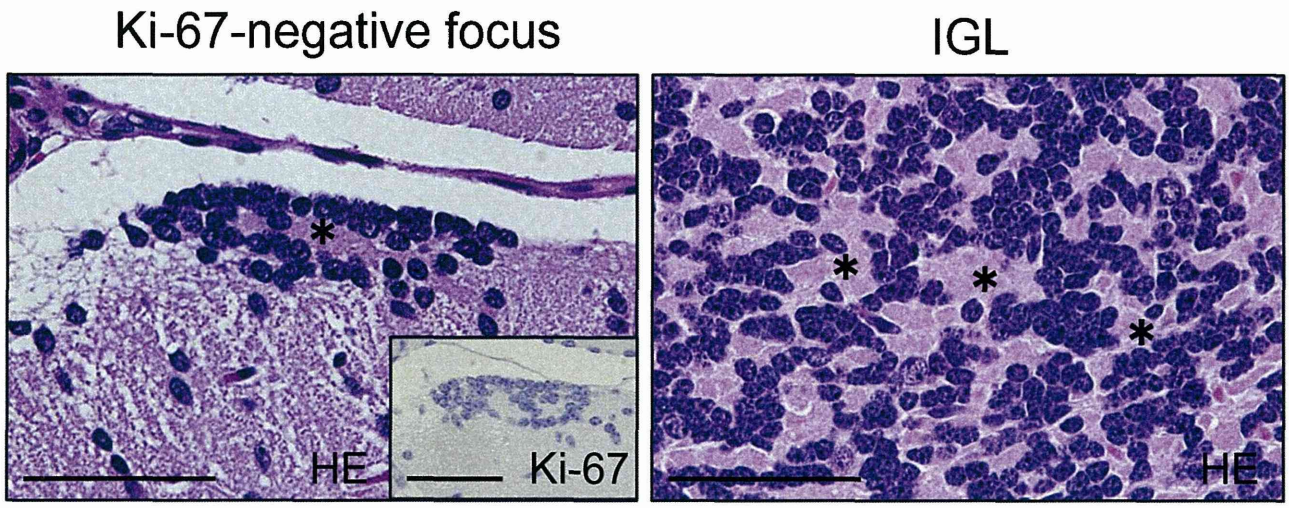

Fig. 8. Ki-67-negative foci showing differentiation into the IGL. HE staining of Ki-67-negative focus (left) and the IGL (right) of Ptch1 mice at PND21. An eosinophilic mossy fiber-like substance (asterisk) was surrounded by nuclei of Ki-67-negative focus. Mossy fibers (asterisk) were observed among the nuclei of granular cells of the IGL. Scale bar: 50 μm.

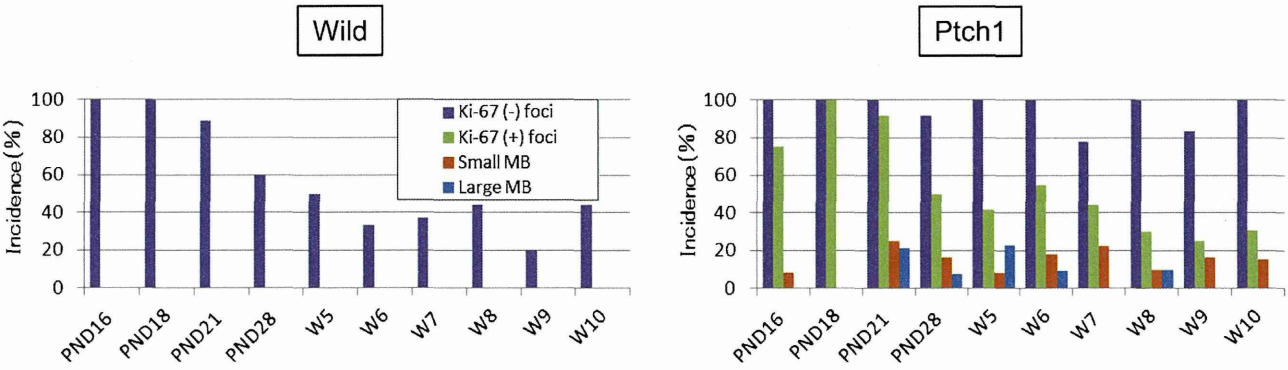

Fig. 9. Incidences of Ki-67-negative (−) and positive (+) foci and MBs in wild-type and Ptch1 mice. Incidences (%) were calculated as follows; number of animals which have specific lesion (e.g. Ki-67-negative foci) in the cerebellum relative to the total number of animals examined. Ki-67-negative foci were observed in both genotypes, but in higher incidence in Ptch1 mice throughout the examination period. The incidence of Ki-67-positive foci had a tendency to decrease with aging. Incidences of small MB and large MB had no tendency to increase with aging.

4. Discussion

The present study was performed to clarify derived cell and early changes of MBs in Ptch1 mice using immunohistochemistry. We also compared cerebellar developmental processes in Ptch1 mice to wild-type mice. Currently, human MBs are classified as four distinct subtypes by molecular studies (Ellison et al., 2011; Northcott et al., 2011; Jones et al., 2012; Kool et al., 2012). Tumors of Ptch1 mice are thought to be equivalent for those of the Shh subgroup in human (Lau et al., 2012). Therefore, MBs in Ptch1 mice will be good tool for testing new drugs targeting the Shh pathway. Additionally, detailed investigation of the cerebellar development and early changes of MB in Ptch1 mice will be beneficial to understanding pathogenesis of human MBs.

During the experimental period, Ptch1 mice showed no clinical signs except development of hydrocephalus and rhabdomyosarcomas in some cases, an outcome that has been previously described (Corcoran and Scott, 2001; Wetmore et al., 2000; Svärd et al., 2009). Although the pathogenesis of hydrocephalus in Ptch1 mice has not been fully understood, impaired cilia function of the ependymal cells might be related (Gavino and Richard, 2011).

The present study demonstrated that a single injection of BrdU was useful in pursuing the sequential migrating process of GCPs from the EGL to the IGL. Similar to results of another study (Thomas et al., 2009), we observed that the migration process in Ptch1 mice was the same as that in wild-type mice and that the proliferation of GCPs increased in Ptch1 mice resulting in a slightly wider EGL layer. No clear evidence was obtained, but the increased proliferation in the EGL in Ptch1 mice might be related to the high potential for MB described below. Shh signaling regulates the expansion of the pool of GCPs (Roussel and Hatten, 2011; Wang et al., 2012). Reduced levels of Ptch1 expression in the cerebellum of Ptch1 mice might be caused by loss of one allele resulting in increased proliferation of GCPs (Corcoran and Scott, 2001; Goodrich et al., 1997; Gupta et al., 2010; Toftgard, 2000; Yang et al., 2008). In addition, an extended duration of GCP localization in the EGL might increase opportunities for additional mutations which may lead to tumorigenesis (Corcoran and Scott, 2001; Wetmore et al., 2000).

Proliferative lesions such as preneoplastic lesions of MBs during 3 weeks after birth in Ptch1 mice were described as rare occurrences in previous reports (Kim et al., 2003); however, our detailed and sequential examination revealed that proliferative lesions and MBs had already been detected in Ptch1 mice within 3 weeks after birth. The morphology and immunohistochemistry of MBs at PND12 indicated that MBs arose from GCPs of the outer layer of the EGL during cerebellar development. The cells of the earliest proliferative lesion, focal thickened area of the EGL, showed the same immunohistochemical profiles as GCPs of the outer layer of the EGL.

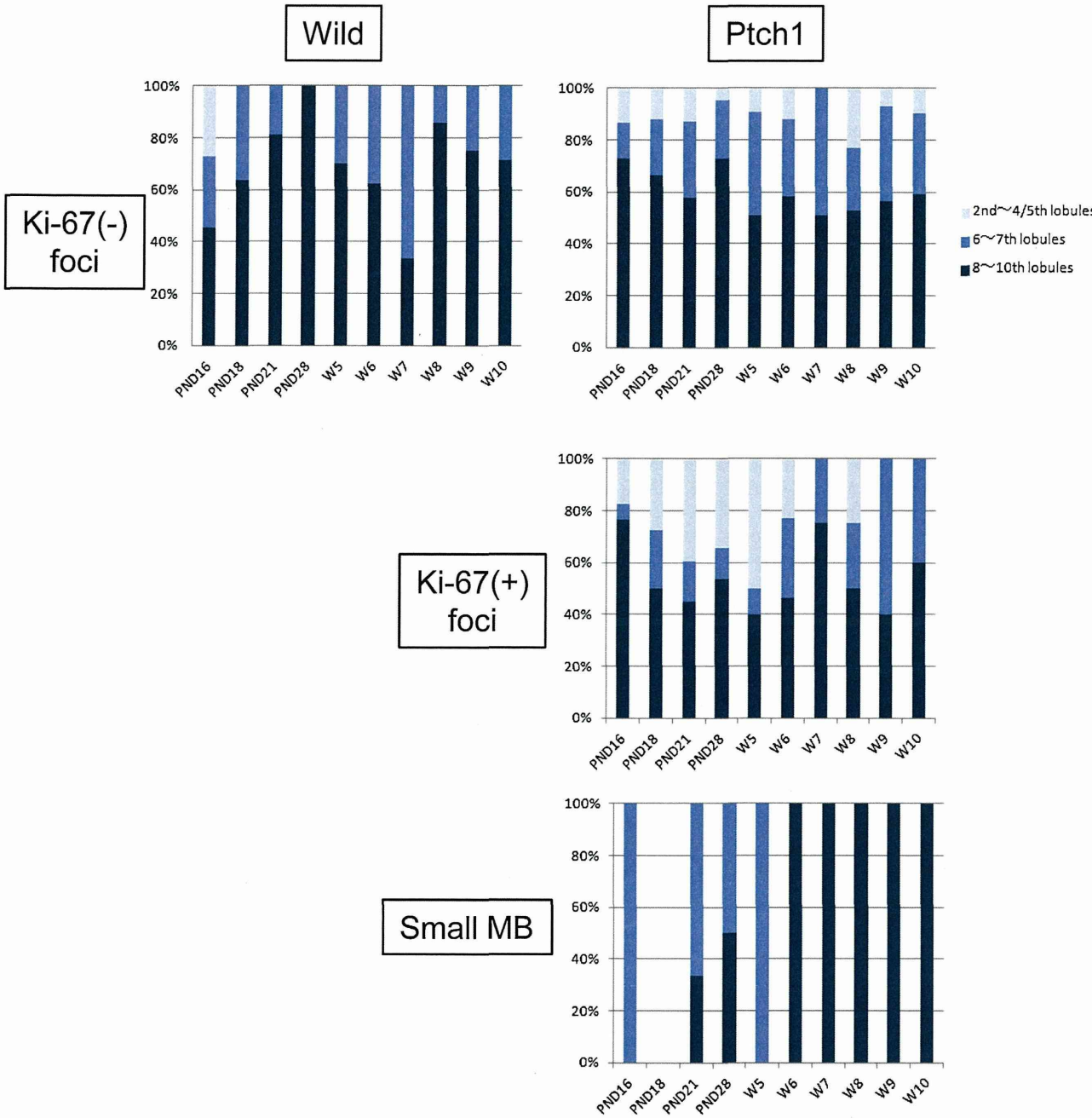

Fig. 10. Location of Ki-67-negative (−) and positive (+) foci and small MBs in the cerebellum of wild-type and Ptch1 mice. Incidences (%) were calculated as follows; total number of specific lesion per cerebellar lobule of all animal examined relative to total number of the lesion in the whole cerebellum of all animals examined.

As the thickened area had cellular atypia and disarrangement compared to normal GCPs, it was considered to be preneoplastic of MB. The appearance of focal thickened proliferative lesions was limited during PND10 to PND14 when the EGL was detectable in this study. It may be that those lesions were recognized as Ki-67-positive foci or small MBs after PND16 because normal GCPs neighboring the lesions disappeared due to migration into the IGL after PND16.

We also found another preneoplastic lesion of MB derived from residual GCPs as Ki-67-positive focus only in Ptch1 mice. In previous reports, MBs were thought to arise from residual GCPs located at the surface of the cerebellum (Corcoran and Scott, 2001; Goodrich et al., 1997). In our study, the foci of GCP-like cells were found on the surface of the cerebellar cortex and only detectable on and after PND16. They were clearly divided into two types by the morphological and immunohistochemical profiles and genotypes. Observation of the EGL in BrdU-treated animal revealed that both types of the foci with BrdU-positive cells were composed of residual GCPs. The cells of Ki-67 positive foci had the same profiles as granular cells of the outer layer of the EGL, indicating that they were undifferentiated and had high proliferating potential. The other focus, Ki-67-negative type, was composed of cells showing neuronal differentiation with a lack of proliferating activity. They resembled granular cells of the IGL or the inner layer of the EGL indicating that the cells were already differentiated into mature granular cells. The Ki-67-negative foci were detected in both genotypes. In addition, more than half of the Ki-67-positive foci were located in the 6–10th lobules of the cerebellum as well as in small MBs in Ptch1 mice. Although MBs are thought to be derived from residual GCPs located in the EGL of the cerebellum (Behesti and Marino, 2009; Roussel and Hatten, 2011), these results strongly suggest that residual GCPs in the Ki-67-positive

foci were preneoplastic lesions. A high yield of Ki-67-positive foci may be useful as an easily detectable and confidential indicator of MB. These preneoplastic lesions might be useful as early markers to detect modulation effects of chemicals to shorten experimental periods.

The observation of a higher incidence of Ki-67-negative foci in Ptch1 mice as compared to wild-type mice and a reduced incidence of Ki-67-negative foci with increased age in wild-type mice was unexpected. These findings may be attributable to smaller Ki-67-negative foci in wild-type mice and a much lower number per animal as compared to Ptch1 mice, although their incidences were 100%. Chances to find the foci in a cross section of the cerebellum may have been reduced with increased age in wild-type mice due to cerebellar growth.

Purkinje cells secrete the mitogen Shh for GCP proliferation in the EGL during early phases of cerebellar development (Roussel and Hatten, 2011). After the GCPs lost cell proliferating activity, they migrate along radial fibers of Bergmann glia (Roussel and Hatten, 2011). It has been reported that abnormal development of Purkinje cells and Bergmann glia can disrupt proliferation, migration, and differentiation of GCPs (Adams et al., 2002; D'Arca et al., 2010; Rakic and Sidman, 1973; Schwartz et al., 1997). Our immunohistochemical results demonstrate no abnormal morphology in Bergmann glia or Purkinje cells, indicating that the MB formation process during cerebellar development might be intrinsic to the GCPs rather than abnormalities in Bergmann glia and Purkinje cells.

In conclusion, a thickened area of the EGL and Ki-67-positive foci were considered to be the early preneoplastic lesions of MBs derived from GCPs in the EGL in Ptch1 mice. These were distinguishable by immunohistochemistry with proliferation and neuronal differentiation markers. Preneoplastic lesions of MBs may serve as useful indicators and as substitutions for advanced MBs in the evaluation of drug efficacy and modulating effects of additional gene mutations, chemicals, and irradiation. Importantly, the Ki-67-positive focus is an easily detectable and confidential indicator due to higher occurrences in the third week after birth.

Acknowledgements

We thank Tomomi Morikawa for technical assistance in conducting the study and genotyping, and Miss Ayako Kaneko for technical assistance in histopathological preparation. This study was partly supported by Health and Labor Sciences Research Grants, Research on Risk of Chemical Substances, Ministry of Health, Labor and Welfare (H22-Toxicol-003).

References

Adams NC, Tomoda T, Cooper M, Dietz G, Hatten ME. Mice that lack astrotactin have slowed neuronal migration. Development 2002;129:965–72.

Aref D, Moffatt CJ, Agnihotri S, Ramaswamy V, Dubuc AM, Northcott PA, et al. Canonical TGF-beta pathway activity is a predictor of SHH-driven medulloblastoma survival and delineates putative precursors in cerebellar development. Brain Pathology 2012.

Ayrault O, Zindy F, Rehg J, Sherr CJ, Roussel MF. Two tumor suppressors, p27Kip1 and patched-1, collaborate to prevent medulloblastoma. Molecular Cancer Research 2009;7:33–40.

Behesti H, Marino S. Cerebellar granule cells: insights into proliferation, differentiation, and role in medulloblastoma pathogenesis. The International Journal of Biochemistry and Cell Biology 2009;41:435–45.

Bhatia B, Potts CR, Guldal C, Choi S, Korshunov A, Pfister S, et al. Hedgehog-mediated regulation of PPARγ controls metabolic patterns in neural precursors and shh-driven medulloblastoma. Acta Neuropathologica 2012;123:587–600.

Briggs KJ, Corcoran-Schwartz IM, Zhang W, Harcke T, Devereux WL, Baylin SB, et al. Cooperation between the Hic1 and Ptch1 tumor suppressors in medulloblastoma. Genes and Development 2008;22:770–85.

Corcoran RB, Scott MP. A mouse model for medulloblastoma and basal cell nevus syndrome. Journal of Neuro-Oncology 2001;53:307–18.

Crawford JR, MacDonald TJ, Packer RJ. Medulloblastoma in childhood: new biological advances. The Lancet Neurology 2007;6:1073–85.

D'Arca D, Zhao X, Xu W, Ramirez-Martinez NC, Iavarone A, Lasorella A. Huwe1 ubiquitin ligase is essential to synchronize neuronal and glial differentiation in the developing cerebellum. Proceedings of the National Academy of Sciences of the United States of America 2010;107:5875–80.

Dhall G. Medulloblastoma. Journal of child neurology 2009;24:1418–30.

Dyer MA. Mouse models of childhood cancer of the nervous system. Journal of clinical pathology 2004;57:561–76.

Ecke I, Rosenberger A, Obenauer S, Dullin C, Aberger F, Kimmina S, et al. Cyclopamine treatment of full-blown Hh/Ptch-associated RMS partially inhibits Hh/Ptch signaling, but not tumor growth. Molecular carcinogenesis 2008;47:361–72.

Ellison DW, Dalton J, Kocak M, Nicholson SL, Fraga C, Neale G, et al. Medulloblastoma: clinicopathological correlates of SHH WNT, and non-SHH/WNT molecular subgroups. Acta Neuropathologica 2011;121:381–96.

Farioli-Vecchioli S, Tanori M, Micheli L, Mancuso M, Leonardi L, Saran A, et al. Inhibition of medulloblastoma tumorigenesis by the antiproliferative and pro-differentiative gene PC3. FASEB Journal 2007;21:2215–25.

Gavino C, Richard S. Patched1 haploinsufficiency impairs ependymal cilia function of the quaking viable mice, leading to fatal hydrocephalus. Molecular and Cellular Neurosciences 2011;47:100–7.

Goodrich LV, Milenkovic L, Higgins KM, Scott MP. Altered neural cell fates and medulloblastoma in mouse patched mutants. Science 1997;277:1109–13.

Gupta S, Takebe N, Lorusso P. Targeting the Hedgehog pathway in cancer. Therapeutic Advances in Medical Oncology 2010;2:237–50.

Hahn H, Wojnowski L, Miller G, Zimmer A. The patched signaling pathway in tumorigenesis and development: lessons from animal models. Journal of Molecular Medicine (Berlin, Germany) 1999;77:459–68.

Haldipur P, Bharti U, Govindan S, Sarkar C, Iyengar S, Gressens P, et al. Expression of Sonic hedgehog during cell proliferation in the human cerebellum. Stem Cells and Development 2012;21:1059–68.

Hatten ME, Roussel MF. Development and cancer of the cerebellum. Trends in Neurosciences 2011;34:134–42.

Huse JT, Holland EC. Targeting brain cancer: advances in the molecular pathology of malignant glioma and medulloblastoma. Nature Reviews Cancer 2010;10:319–31.

Jones DT, Jager N, Kool M, Zichner T, Hutter B, Sultan M, et al. Dissecting the genomic complexity underlying medulloblastoma. Nature 2012;488:100–5.

Kim JY, Nelson AL, Algon SA, Graves O, Sturla LM, Goumnerova LC, et al. Medulloblastoma tumorigenesis diverges from cerebellar granule cell differentiation in patched heterozygous mice. Developmental Biology 2003;263:50–66.

Kimura H, Stephen D, Joyner A, Curran T. Gli1 is important for medulloblastoma formation in $Ptc1^{+/-}$ mice. Oncogene 2005;24:4026–36.

Klesse LJ, Bowers DC. Childhood medulloblastoma: current status of biology and treatment. CNS Drugs 2010;24:285–301.

Kool M, Korshunov A, Remke M, Jones DT, Schlanstein M, Northcott PA, et al. Molecular subgroups of medulloblastoma: an international meta-analysis of transcriptome, genetic aberrations, and clinical data of WNT, SHH, Group 3, and Group 4 medulloblastomas. Acta Neuropathologica 2012;123:473–84.

Lau J, Schmidt C, Markant SL, Taylor MD, Wechsler-Reya RJ, Weiss WA. Matching mice to malignancy: molecular subgroups and models of medulloblastoma. Child's Nervous System 2012;28:521–32.

Mohan AL, Friedman MD, Ormond DR, Tobias M, Murali R, Jhanwar-Uniyal M. PI3K/mTOR signaling pathways in medulloblastoma. Anticancer Research 2012;32:3141–6.

Northcott PA, Korshunov A, Witt H, Hielscher T, Eberhart CG, Mack S, et al. Medulloblastoma comprises four distinct molecular variants. Journal of Clinical Oncology 2011;29:1408–14.

Oliver TG, Read TA, Kessler JD, Mehmeti A, Wells JF, Huynh TT, et al. Loss of patched and disruption of granule cell development in a pre-neoplastic stage of medulloblastoma. Development 2005;132:2425–39.

Pazzaglia S. Ptc1 heterozygous knockout mice as a model of multi-organ tumorigenesis. Cancer Letters 2006;234:124–34.

Pazzaglia S, Pasquali E, Tanori M, Mancuso M, Leonardi S, di Majo V, et al. Physical, heritable and age-related factors as modifiers of radiation cancer risk in patched heterozygous mice. International Journal of Radiation Oncology, Biology, Physics 2009;73:1203–10.

Pazzaglia S, Tanori M, Mancuso M, Gessi M, Pasquali E, Leonardi S, et al. Two-hit model for progression of medulloblastoma preneoplasia in Patched heterozygous mice. Oncogene 2006;25:5575–80.

Pogoriler J, Millen K, Utset M, Du W. Loss of cyclin D1 impairs cerebellar development and suppresses medulloblastoma formation. Development 2006;133:3929–37.

Raffel C. Medulloblastoma: molecular genetics and animal models. Neoplasia 2004;6:310–22.

Rakic P, Sidman RL. Weaver mutant mouse cerebellum: defective neuronal migration secondary to abnormality of Bergmann glia. Proceedings of the National Academy of Sciences of the United States of America 1973;70:240–4.

Roussel MF, Hatten ME. Cerebellum development and medulloblastoma. Current Topics in Developmental Biology 2011;94:235–82.

Schwartz PM, Borghesani PR, Levy RL, Pomeroy SL, Segal RA. Abnormal cerebellar development and foliation in $BDNF^{-/-}$ mice reveals a role for neurotrophins in CNS patterning. Neuron 1997;19:269–81.

Svärd J, Rozell B, Toftgard R, Teglund S. Tumor suppressor gene co-operativity in compound Patched1 and suppressor of fused heterozygous mutant mice. Molecular Carcinogenesis 2009;48:408–19.
Takahashi M, Matsuo S, Inoue K, Tamura K, Irie K, Kodama Y, et al. Development of an early induction model of medulloblastoma in Ptch1 heterozygous mice initiated with N-ethyl-N-nitrosourea. Cancer Science 2012;103:2051–5.
Thomas WD, Chen J, Gao YR, Cheung B, Koach J, Sekyere E, et al. Patched1 deletion increases N-Myc protein stability as a mechanism of medulloblastoma initiation and progression. Oncogene 2009;28:1605–15.
Toftgard R. Hedgehog signalling in cancer. Cellular and Molecular Life Sciences 2000;57:1720–31.
Uziel T, Zindy F, Xie S, Lee Y, Forget A, Magdaleno S, et al. The tumor suppressors Ink4c and p53 collaborate independently with Patched to suppress medulloblastoma formation. Genes and Development 2005;19:2656–67.
Wang X, Venugopal C, Manoranjan B, McFarlane N, O'Farrell E, Nolte S, et al. Sonic hedgehog regulates Bmi1 in human medulloblastoma brain tumor-initiating cells. Oncogene 2012;31:187–99.
Wetmore C, Eberhart DE, Curran T. The normal patched allele is expressed in medulloblastomas from mice with heterozygous germ-line mutation of patched. Cancer Research 2000;60:2239–46.
Wetmore C, Eberhart DE, Curran T. Loss of p53 but not ARF accelerates medulloblastoma in mice heterozygous for patched. Cancer Research 2001;61:513–6.
Wu X, Northcott PA, Croul S, Taylor MD. Mouse models of medulloblastoma. Chinese Journal of Cancer 2011;30:442–9.
Yang ZJ, Ellis T, Markant SL, Read TA, Kessler JD, Bourboulas M, et al. Medulloblastoma can be initiated by deletion of Patched in lineage-restricted progenitors or stem cells. Cancer Cell 2008;14:135–45.

Toxicologic Pathology, 41: 1011-1015, 2013

ISSN: 0192-6233 print / 1533-1601 online
DOI: 10.1177/0192623313476575

Vascular Hamartoma in the Uterus of a Female Sprague-Dawley Rat with an Episode of Vaginal Bleeding

Mariko Shirota[1], Jun Kawashima[1], Tomohiro Nakamura[1], Yuko Ogawa[1], Junichi Kamiie[2], and Kinji Shirota[2]

[1]*Laboratory of Comparative Toxicology, Azabu University, Sagamihara, Japan*
[2]*Laboratory of Veterinary Pathology, Azabu University, Sagamihara, Japan*

Abstract

An annular, reddened lesion with mild serosal hemorrhage and no tumorous mass formation was detected in the right uterine horn of a 37-week-old female Sprague-Dawley rat that had postpubertal vaginal bleeding. Histological examination revealed prominent proliferation of the endometrium, which occupied the uterine lumen. There were numerous aberrant vascular spaces filled with erythrocytes, proliferation of stromal cells, and inflammatory infiltrates including hemosiderin-laden macrophages in the endometrium. These vasculatures extended into the myometrium, and in a transverse section of the lesion, they were mostly distributed throughout the circumference of the uterus. They were irregular in shape and interconnected, forming a large vascular sinus and anastomosing reticular channels. In the area with serosal hemorrhage, the muscular layer covering the large irregular vascular space had undergone degeneration and necrosis. The lining cells of the vasculatures were often plump, and they protruded into the lumen and were arranged in a tombstone or hobnail manner. Immunostaining revealed that these cells were positive for von Willebrand factor and CD34. The aberrant vasculatures were not accompanied by pericytes or muscular layer, although a discontinuous muscular wall was present around some of them. From these results, the uterine lesion was diagnosed as a vascular hamartoma.

Keywords: histopathology; rat pathology; reproductive system; vascular system.

Introduction

Spontaneous vascular tumors are not common in laboratory rats, although hemangiomas, hemangiosarcomas, hemangiopericytomas, and lymphangiosarcomas have been detected in aged control rats in carcinogenicity studies. The first 2 of these tumors have been found in the spleen, lymph nodes, liver, skin, heart, blood vessels, abdominal cavity, cranial cavity, thoracic cavity, eye, kidney, testis, vagina, and uterus (Baldrick 2005; Brix et al. 2005; Chandra, Riley, and Johnson 1992; Dinse et al. 2010; Goodman et al. 1979; Keenan et al. 1995; McMartin et al. 1992; Nakazawa et al. 2001; Zwicker et al. 1995). Among these organs, the spleen, skin, and lymph nodes are the most common sites of these tumors. The overall incidence of the hemangiomas and hemangiosarcomas in control animals in 2-year carcinogenicity tests with Sprague-Dawley (SD) rats are 0.19 to 0.5% and 0.3 to 0.9%, respectively (Brix et al. 2005; Chandra, Riley, and Johnson 1992; Dinse et al. 2010; McMartin et al. 1992; Zwicker et al. 1995). With regard to the age of rats with these tumors, Zwicker et al. (1995) observed 8 cases of hemangiomas in rats with an average age of 658 days (range, 565–735) and 5 cases of hemangiosarcomas in rats with an average age of 685 days (range, 638–728) in SD rats. In a report by McMartin et al. (1992), hemangiopericytomas occurred in 0.2% of females and 0% of males, and lymphangiosarcomas occurred in 0.2% of males and 0% of females of aged control SD rats (585 of each sex).

Vascular uterine tumors have been rarely reported in aged SD rats, and none have been recorded in Fischer 344 rats (Dinse et al. 2010; Goodman et al. 1979) or Wistar rats (Poteracki and Walsh 1998). A uterine hemangioma was found in 1 of the 710 female SD rats (Zwicker et al. 1995) and 1 of the 350 female SD rats (Keenan et al. 1995). However, the incidence of uterine hemangiosarcomas has been reported to be 0.08% of 1,329 female SD rats (Chandra, Riley, and Johnson 1992). In humans, vascular uterine tumors are very rare, and they may cause uterine bleeding (Sharma et al. 2006; Virk, Zhong, and Lu 2009; Weissman, Talmon, and Jakobi 1993).

In this article, we describe the histological features and have discussed the nature of the aberrant and localized vascular proliferative lesions that were detected in the uterine horn of an adult female SD rat that experienced a postpubertal episode of vaginal bleeding.

Case Report

The animal was a 37-week-old female SD rat (CrJ:CD; Charles River Japan Inc., Kanagawa, Japan) that received a single subcutaneous administration of 7 μl of 17α-ethynyl estradiol (EE, Sigma-Aldrich Corporation, St. Louis, MO) that was concentrated in 0.08 μg/ml 1 day after birth; 4 other littermates received a similar administration. The rats were housed

The author(s) declared no potential conflicts of interest with respect to the research, authorship, and/or publication of this article.

The author(s) disclosed receipt of the following financial support for the research, authorship, and/or publication of this article: This study was partly supported by a grant in aid for research on risk of the origin of chemical compounds from the Minister of Health, Labor and Welfare (H22-Kagaku-Ippan-003).

Address correspondence to: Kinji Shirota, Laboratory of Veterinary Pathology, Azabu University, 1-17-71 Fuchinobe, Chuo-ku, Sagamihara, Kanagawa 252-5201, Japan; e-mail: shirota@azabu-u.ac.jp.

Abbreviations: α-SMA, α-smooth muscle actin; H&E, hematoxylin and eosin; PCNA, proliferating cell nuclear antigen; SD, Sprague-Dawley; vWF, von Willebrand factor.

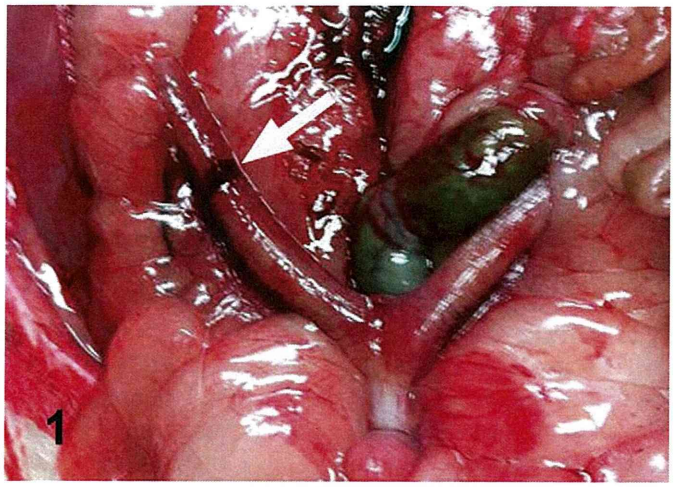

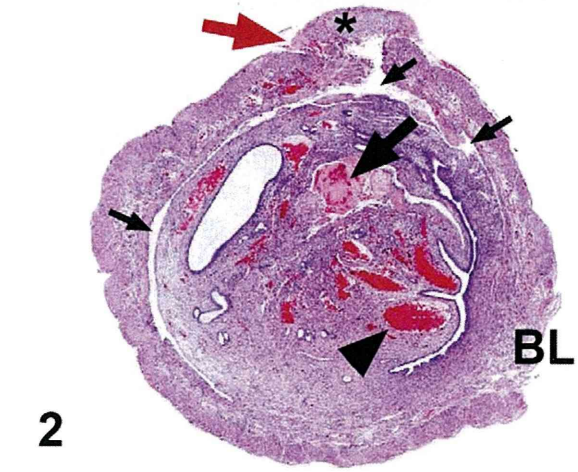

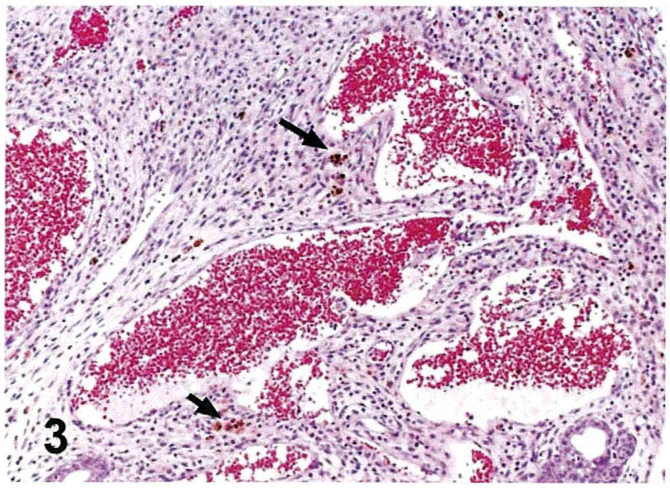

FIGURE 1.—Macroscopic feature of the lesion in the right uterine horn (white arrow). FIGURE 2.—Low-power views of the microscopic features of the uterine lesion. Endometrial proliferation occludes the uterine lumen. There are many cavernous vascular spaces filled with red blood cells (arrow head). The large arrow indicates a thrombus in the irregularly dilated vascular lumen. Long, irregular vascular spaces along the muscular layers cover two-third of the uterine circumference on a transverse section (small arrows). The asterisk indicates degeneration of uterine wall. A higher magnification image of the lesion indicated by the red arrow is shown in Figure 5. H&E (1×).

in a barrier system animal facility with a 12-hr light/dark cycle, a temperature of 21 ± 1°C, and a relative humidity of 50 to 60%. The rats were fed a CLEA Rodent Diet CE-2 (CLEA Japan, Inc., Tokyo, Japan), and they had free access to tap water. A 14-day evaluation of vaginal smears was performed every 4 weeks from 8 weeks of age. At 28 weeks of age, vaginal bleeding was detected in one of the rats. Therefore, smear sampling was stopped, and bleeding was observed until 32 weeks of age. Vaginal smear evaluation revealed recurrent estrus that occurred in 4- or 5-day cycles until the start of bleeding. Smear sampling was restarted at 35 weeks of age, and no bleeding was observed for 2 weeks. At 37 weeks of age, the rat was deeply anesthetized with sodium pentobarbital (Somnopentil, Kyoritsu Shoji Co., Tokyo, Japan) and euthanized by postcava bleeding. All procedures in this study were performed in accordance with the guidelines approved by the Animal Research Committee of our institution.

At necropsy, the body weight was 554 g, and no external abnormalities were observed. However, an annular reddened lesion 3 mm wide with a slight serosal hemorrhage was found in the right uterine horn with no mass formation (Figure 1). There were no gross abnormalities in any other organs. The systemic tissues, including the uterus, were excised, fixed in 10% phosphate-buffered neutral formalin, and embedded in paraffin according to a routine method. Serial paraffin sections were prepared and stained with hematoxylin and eosin (H&E); some sections were used for immunostaining. In addition, sections from other systemic organs were stained with H&E for light microscopy. Immunostaining was performed with an immunoenzyme polymer method with goat anti-rat CD34 (R&D Systems, Inc., Minneapolis, MN), rabbit anti-human von Willebrand factor (vWF) antibody (DAKO Denmark A/S, Glostrup, Denmark), mouse anti-human α-smooth muscle actin (α-SMA) antibody (clone 1A4; DAKO Denmark A/S), and mouse antiproliferating cell nuclear antigen (PCNA) antibody (clone PC10; DAKO Denmark A/S) as primary antibodies. The immunoreaction was visualized by peroxidase-conjugated anti-goat immunoglobulin (Ig; Histofine Simple Stain MAX-PO (G); Nichirei Biosciences Inc., Tokyo, Japan), peroxidase-conjugated anti-rabbit Ig (Histofine Simple Stain MAX-PO (R); Nichirei Biosciences Inc.) or peroxidase-conjugated anti-mouse Ig (Histofine Simple Stain MAX-PO (M); Nichirei Biosciences Inc.), and 3,3′-diaminobenzidine. In all immunostainings, Mayer's hematoxylin was used for counterstaining.

Light microscopic examination of the uterine lesion revealed prominent proliferation of the endometrium, which mostly occupied the uterine lumen. There were many aberrant cavernous vascular spaces filled with erythrocytes, occasionally accompanied by thrombi (Figure 2). In addition, diffuse proliferation of spindle stromal cells and infiltration of eosinophils, neutrophils, lymphocytes, and hemosiderin-laden

FIGURE 2. (Continued). BL = broad ligament of the uterus. FIGURE 3.—Cavernous vascular spaces in the endometrium with intense stromal cell proliferation and cellular infiltration, including hemosiderin-laden macrophages (arrows). H&E (100×).

macrophages were observed in the endometrium (Figure 3). Necrosis and desquamation of the endometrial epithelium were not found. The irregular vascular spaces extended from the endometrium to the myometrium and were distributed over nearly two-third of the uterine circumference on a transverse section, as shown in Figure 2. Examination of the serial sections revealed that these vasculatures were prominently irregular in shape and interconnected, and they formed a large vascular sinus or anastomosing reticular vascular channels (Figure 2). In the area with serosal hemorrhage (Figure 2), the muscular layer covering the large irregular vascular space had undergone degeneration and necrosis with proliferation of fibroblasts and infiltration of macrophages, resulting in perforation of the uterine wall and serosal hemorrhage (Figures 4 and 5). The lining cells of the endometrial cavernous spaces were mostly flat (Figure 3), while those of other aberrant vasculatures found throughout the uterine wall were often cuboidal or plump. They protruded into the lumen and were arranged in a tombstone or hobnail manner (Figure 6). In some lumens, the lining cells were plump and protruded into the lumens, but they were flat as those in the normal vessels on the other side (Figure 7). Mitosis was not detected in the flat endothelial cells and was rarely found in the plump lining cells.

Immunohistochemical examination revealed that the lining cells of the aberrant vasculatures were positive for vWF (Figure 8A) and CD34 (Figure 8B). However, immunoreactivity for vWF was less intense than that in normal endothelial cells. Staining for PCNA was frequently positive in the lining cells of the aberrant vasculatures (Figure 8C), whereas normal endothelial cells were positive only occasionally. In addition, endometrial epithelium and stromal cells, myometrial cells, and fibroblasts were frequently positive for PCNA. Normal blood vessels in the lesion were encircled by α-SMA-positive pericytes or smooth muscle layers. The aberrant vasculatures were not accompanied by α-SMA-positive pericytes or muscular layer, although discontinuous muscular walls had formed around some abnormal vessels (Figure 9).

The aberrant vasculatures were localized to the portion of the uterine horn that corresponded to the gross annular lesion. No abnormalities were found in any of the other uterine tissues, including the opposite uterine horn, ovaries, or other systemic organs. The littermates of the experimental rat did not show any lesions in their main organs, including the uterus.

The results of immunohistochemical examination suggested that the lining cells of the aberrant vasculatures in the uterine lesion were vascular endothelial cells with high proliferative activity. In rats, an endometrial stromal polyp, which is often highly vascular throughout the stroma, is sometimes termed an angiomatous polyp (Goodman and Hildebrandt 1987). A cavernous hemangiomatous polyp (Sharma et al. 2006) is accompanied by many neoplastic vasculatures in the endometrium. However, the structure and distribution of the aberrant vasculatures observed in the present case were different from those previously recorded in human and rat uterine tumors (Dixon et al. 1999).

The present case and its littermates were administered 17α-ethynyl estradiol 1 day after birth. Estrogen induces vascular endothelial growth factor in the uterus, which promotes vascular growth and increases vascular permeability (Cullinan-Bove and Koos 1993). However, no uterine vascular lesions were found in the littermates of the present case, and those rats in the other experiment performed by our group received doses of 17α-ethynyl estradiol that were the same or higher (Shirota et al. 2012). In addition, the lesion was localized to a limited portion of the uterine horn. These findings obviously indicated that there were no close relationship between the 17α-ethynyl estradiol administered and the development of the uterine lesion.

In general, neoplastic vasculatures form massive or nodular lesions in both benign and malignant tumors. In contrast, the uterine lesion in this case did not form a tumorous mass. The aberrant vasculatures showed cavernous, sinusoidal, or incomplete venous appearances. They extended throughout the uterine wall and expanded to nearly the entire circumference of the affected site of the uterine horn, but they were unlikely to have been invasive, destructive, or compressive. In addition, cavernous or sinusoidal structures were not associated with α-SMA-positive pericytes, and some vasculatures had discontinuous muscular walls. Heterogeneity of the vasculatures composing a lesion is observed in some vascular hamartomas (Sugiyama et al. 2007; Yasuno et al. 2011) or congenital vascular abnormalities (Booler 2008; Redondo 2007), but not in vascular tumors (Calonje and Flecher 2007). As per these histological features of the uterine vasculatures, the lesion in the present case might be a vascular malformation rather than a true neoplasia.

The term vascular hamartoma, which has preferentially been used in veterinary pathology, is used as a synonym of vascular malformation in human pathology (Calonje and Flecher 2007). Human vascular malformations are benign non-neoplastic lesions, which are present from birth and often grow slowly during a lifetime (Redondo 2007). Most vascular tumors in rats have been found in aged control animals from 2-year carcinogenicity studies (Brix et al. 2005; Keenan et al. 1995). In addition, no vascular tumors have been detected in these studies in rats aged about 22 to 60 weeks by interim necropsy. The present case was 37 weeks of age, and fairly young compared with the rats with vascular tumors. Accordingly, the vascular lesion in the uterus was finally diagnosed as a vascular hamartoma. Expression of PCNA, which is frequently observed in nonendothelial cells in the uterus, might not be related to the vascular abnormalities, but might instead reflect the physiological conditions in the estrous cyclicity of the rat. The rat had a postpubertal episode of vaginal hemorrhage, which might have been related to the vascular lesion of the uterus.

There have been several reports of vascular hamartoma in animals (Calonje and Flecher 2007), and these studies illustrated the diverse morphology of vascular lesions in dogs (Beccaglia et al. 2008; Booler 2008; Corzo-Menendez et al. 2011; Smith and Van Winkle 2001; Yasuno et al. 2011), cattle (Benoit et al. 2005; Sugiyama et al. 2007), and a cat (Parkes et al. 2009). This report might be the first of a vascular hamartoma in a rat.